The Two Components in the Distribution of Sunspot Groups with Respect to their Maximum Areas

M. H. Gokhale and K. R. Sivaraman *Indian Institute of Astrophysics, Bangalore 560034*

Abstract. From an analysis of the distribution of sunspot groups with respect to their maximum areas we find that this distribution consists of two distinct components. One component contributes to spot groups of all possible values of A_* with a distribution density varying as ~ exp $(-b_1 \, A_*^{1/2})$ with b_1 nearly constant from cycle to cycle and having a mean value ~10^{-4} km^{-1}. The other component is predominantly responsible for spot groups with $A_* \lesssim 30 \times 10^{-6}$ hemisphere but may provide a few spot groups even above 50×10^{-6} hemisphere. This component may follow a distribution density ~ exp $(- b_2 \, A_*)$. We also determine the widths of the latitude zones over which spot groups in various intervals of A_* appear and study their variation with time. These widths and their variations indicate that the two statistical samples of spot groups may be produced by two families of flux-tube clusters as suggested earlier in a phenomenological model. Very thin flux-tube clusters in the statistical samples seem to be related to the ephemeral active regions and X-ray bright points.

Key words: sunspots, distribution of areas—solar activity—solar cycle—solar magnetic field

1. Introduction

Studies of the distributions of sunspot groups with respect to their physical properties provide valuable guidelines for the development of models of solar activity and solar magnetic cycle. The distribution of spot groups with respect to the maximum values of their individual areas is especially important for making models based on emergence of magnetic flux tubes or flux ropes. Mandrykina (1974) examined this distribution and showed that the relative frequency of small spot groups is larger during solar minimum than during solar maximum. Lopez Arroyo (1965) and

recently Kuklin (1980) have attempted to fit mathematical expressions for the observed distribution. Motivation for our present study of this distribution is provided by a phenomenological model of the solar cycle proposed earlier by one of us (Gokhale 1977, 1979). According to this model the solar activity during each cycle is provided by two topologically distinct sets of magnetic flux-tube clusters. One set consists of newly formed deep-rooted compact magnetic structures and the other consists of shredded, thin remnants of the 'older' fields in the shallower parts of the convection zone. This model can account for the main qualitative features of the two 'peaks' detected by Gnevyshev (1977) in various parameters of the solar activity (Gokhale 1979). However, a direct verification for the presence of two distinct sets of flux ropes should be sought in the distribution of active regions with respect to the cross-sections of the flux ropes (or flux-tube clusters) that produce the active regions. In the case of conventional active regions, *viz.* those which produce observable pores and spots, the maximum area A_{max} reached by a spot group during its evolution may be taken as a satisfactory measure of the sub-photospheric cross-section of the flux rope responsible for the active region. The maximum area A_{max} may be further approximated by the maximum value A_* among the appropriately corrected observed values of the spot group area. We have studied the frequency distribution $f(A_*)$ of spot groups during each of the last eight solar cycles (1889–1976), using the data from the Greenwich Photoheliographic Results. We find (Section 2) that during each of these eight cycles, the distribution $f(A_*)$ has two components. The first component $f_1(A_*)$ contributes spot groups with all possible values of A_*, whereas the second component $f_2(A_*)$ contributes predominently spot groups of $A_*, \lesssim$ 30 millionths of hemisphere (henceforth expressed as mh).

To examine whether the ensembles of spot groups represented by $f_1(A_*)$ and $f_2(A_*)$ have different physical behaviours, we determine the widths of the latitude zones over which spot groups belonging to different intervals of A_* emerge. The variations of these widths in the solar cycle suggest that the statistical ensembles do correspond to two sets of magnetic flux ropes which differ both in the latitudinal distribution and in the epochs at which they start emerging above the photosphere.

2. The two components in the distribution

2.1 *Method of Analysis*

In Ledgers I and II of the Greenwich Photoheliographic Results, areas (A) of important spot groups as observed from day to day and corrected for foreshort-ening are given for all non-recurrent and recurrent groups observed for two or more days during the years 1894 to 1955. From these we noted down the maximum values A_* of A for each of these spot groups. For each recurrent spot group the highest value of A during its entire life was taken for A_*. For the years 1889 to 1893, when Greenwich Photoheliographic Results do not contain a separate ledger for recurrent spot groups, the identification was done following the well known rotation periods appropriate for the latitudes concerned. For spot groups whose evolution is not included even in Ledger I (and in the case of *all* spot groups from 1956 onwards when Greenwich discontinued providing separate ledgers) the value

of A_* was determined by following the evolution of each spot group from the day-to-day records. For one-day spot groups the area A_0 at the time of observation itself was taken as A_*. Thus values *of A_** were noted down for all spot groups for each year from 1889 to 1976.

The values of A_* so obtained from photoheliograms taken once a day are bound to be different from the true maximum, values (A_{max}) of the area which may be reached in-between two successive observations. However, the difference ($A_{max} — A_*$) can be ignored so long as it is small compared to the width of the interval dA_* chosen for defining the frequency of the distribution. This is ensured by choosing the intervals dA_* at least as large as the magnitude of the typical variation of spot group area during a day. Obviously this requires different widths for dA_* corresponding to the different ranges of A_* values as described later in this paper.

In the case of short-lived spot groups lasting for less than a day, the approximation of A_{max} by the observed value A_0 would be satisfactory if $(A_{max} - A_0) \lesssim 5$ mh which is the halfwidth of the interval dA_* chosen for defining the frequency of small spot groups. This condition will be satisfied in the majority of such spot groups as they are observed in their phase of decay and the average decay rate of solar magnetic features is ~ 10^{15} Mx s^{-1} (Stenflo 1976), *i.e.* ~ 3 mh day^{-1}. Thus the uncertainty in taking A_0 as A_{max} may be tolerated except for 'too small' groups (those with $A_0 \lesssim 10$ mh). A greater uncertainty arises in the counts of small spot groups because they are short-lived and hence some of them will be totally missed in the observations made only once a day. The number of spot groups so missed might even be larger than the observed number for $A_* \lesssim 10$ mh, but for $A_* > 10$ mh the number of 'missed' spot groups may be ignored.

From the yearly values of A_*, frequencies of occurrence $N(A_*, dA_*)$ in intervals of sizes dA_* centred on prescribed values of A_* are now determined. The intervals chosen are as follows.

0–10, 10–20, … 90–100	in the range of 0–100 mh,
75–100, 100–125, … 175–200	in the range 75–200 mh, and
100–200, 200–300, … 900–1000	in the range 100–1000 mh,

All 'closed' at the upper extremity for the sake of definiteness. Number of spot groups with $A_* > 1000$ mh were classified separately. For each interval, the total frequency for each solar cycle was determined by summing up the yearly frequencies for all the years in the cycle.

2.2 *The Distribution Density Function*

The observed values

The observed frequencies $N(A_*, dA_*)$ were divided by widths dA_* of the respective intervals to derive the 'observed values' of the distribution density $f(A_*)$ corresponding to the midpoints A_* of the prescribed intervals. For each solar cycle, the values of $f(A_*)$, were plotted against A_*. These plots are all similar in appearance. Fig. 1 shows $f(A_*)$ for the cycle 1965–1976 as a typical sample. Each plot shows
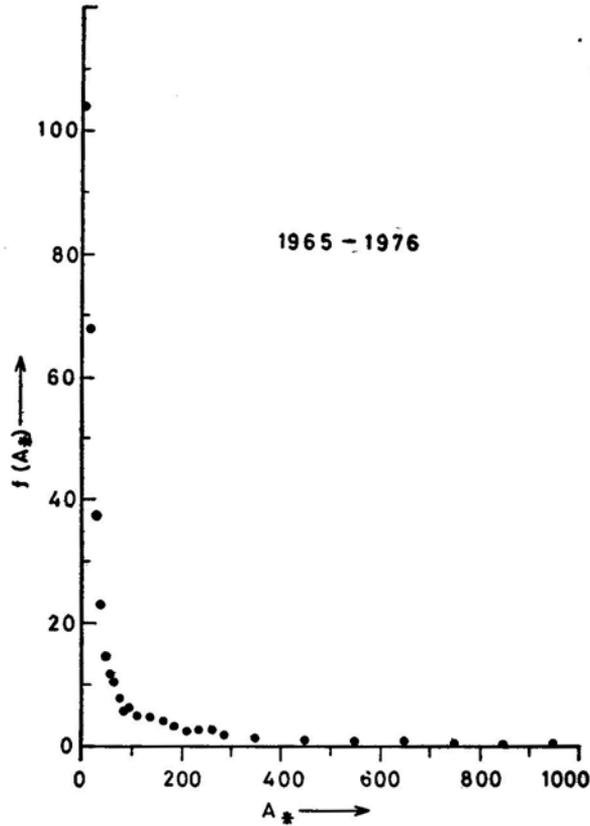
Figure 1. Observed distribution density $f(A)$ mh^{-1} as a function of A_* mh during the cycle 1965–1976.

a 'vertical branch' in the range $A_* < 50$ mh and a 'horizontal branch' for $A_* > 300$ mh which becomes irregular for $A_* > 1000$ mh. All attempts to fit both the branches by a single mathematical term involving a few parameters have failed.

Fit for the 'horizontal branch'

Omitting the frequencies for $A_* > 1000$ mh which are too small for statistical analysis, the horizontal branch fits the expression

$$f_1(A_*) = D_1 \exp\left(-b_1 A_*^{1/2}\right) \tag{1}$$

to a high level of confidence. The same expression continues to hold in the range $A_* < 300$ mh and past $A \sim 100$ mh. We calculated the weighted least square fits for the data in the range 100–1000 mh using formula (1). The values of D_1 and b_1, and the values of the coefficient of correlation $|R_1|$ between ln $[N(A_*, DA_*)]$ and A_* are presented in Table 1. In the same table we have also given the probabilities of χ^2 for each fit. Values outside the brackets correspond to statistical weight based on uncertainties $\sim N^{1/2}$ in the observed frequencies N. Values within the brackets cor-

Table 1. Properties of the component $f_1(A_*)$. Values of D_1 and b_1 and their uncertainties $\sigma(D_1)$, $\sigma(b_1)$ are derived from weighted least-square fits assuming values of A_* to be exact and uncertainties of $\sim N^{1/2}$ in the values of N. Corresponding values of the coefficient of correlation ($|R_1|$) between [$\ln f_1(A_*)$] and $A_*^{1/2}$ are also given for each cycle. Values in brackets correspond to weighted least-square fits assuming the values of N to be exact and uncertainties of $\sim dA_*/2$ in A_* values. The probabilities of χ^2 are derived from the calculated and the observed values of $N(A_*, dA_*)$, and happen to be the same for both methods of fitting.

First component	1889–1901	1902–1913	1914–1923	1924–1933	1934–1944	1945–1954	1955–1964	1965–1976
$D_1 \pm \sigma(D_1)$ mh^{-1}	2287 ± 3	1819 ± 5	2827 ± 7	1858 ± 7	2781 ± 4	2900 ± 4	3573 ± 4	3098 + 4
	(2309 ± 4)	(1967 ± 4)	(2987 ± 5)	(2004 ± 4)	(2780 ± 5)	(2845 ± 3)	(3598 ± 6)	(3724 ± 5)
$b_1 \pm \sigma(b_1)$ mh$^{-1/2}$	0·1608	0·1663	0·1795	0·1626	0·1521	0·1556	0·1589	0·1686
	± 0·0031	± 0·0062	± 0·0070	± 0·0074	± 0·0031	± 0·0033	± 0·0035	± 0·0031
	(0·1623	(0·1705	(0·1835	(0·1659	(0·1627	(0·1559	(0·1607	(0·1700
	± 0·0009)	± 0·0012)	± 0·0012)	± 0·0011)	± 0·0011)	± 0·0007)	± 0·0010)	± 0·0010)
$|R_1|$	0·998	0·994	0·993	0·992	0·998	0·997	0·998	0·998
	(0·997)	(0·991)	(0·994)	(0·995)	(0·998)	(0·998)	(0·997)	(0·997)
χ^2 probability (per cent)	99	82	65	81	9	96	85	92

respond to statistical weights based on uncertainties $\sim dA_*/2$ in A_*. It is interesting to note that the values of b_1 are roughly constant from cycle to cycle, with a mean value $\simeq 0.1643$ mh$^{-1/2}$ *i.e.* $\sim 10^{-4}$ km^{-1} and a root mean square deviation $\simeq 0.0069$ mh$^{-1/2}$.

Comparison with the log-normal law of distribution

Lopez Arroyo (1965) attempted to fit the cumulative frequencies of spot groups by the log-normal law of distribution. The fits obtained by him are rather unimpressive. The χ^2 probabilities exceeded 50 per cent for only five out of fourteen data sets. This is probably because he ignored the large uncertainties in the determination of frequencies for $A_* < 50$ mh and $A_* > 1000$ mh, which could lead to wrong values for percentages of cumulative frequencies. The relative values of cumulative frequencies in the domain 100–1000 mh may not be seriously affected by these uncertainties. We, therefore, fitted the log-normal law of distribution to the values of $f(A_*)$ in this domain. We find that the fit of the log-normal distribution over this range is still poor. However, over the shorter range 300–1000 mh the χ^2 probabilities are 96, 88, 60, 45, 83, 80, 70 and 75 per cent respectively. These probabilities show that the lognormal distribution might at best provide an approximate description of the distribution in the domain 300–1000. It is obvious that the formula (1) is decidedly better both in the coverage of A_* and in χ^2 probabilities.

The second component

In the domain $A_* < 50$ mh the frequencies $N_1(A_*, dA_*)$ calculated from formula (1) fall appreciably below the observed frequencies $N(A_*, dA_*)$. For $A_* \lesssim 30$ mh the difference $N(A_*, dA_*) - N_1(A_*, dA_*)$ is larger than $N_1(A_*, dA_*)$ and keeps increasing as A_* decreases. This indicates that the distribution function $f(A_*)$ must contain another term $f_2(A_*)$ which contributes substantially for $A_* \lesssim 50$ mh and very little for $A_* > 50$ mh.

We estimated the values of $f_2(A_*)$ for each cycle from the expression

$$f_2(A_*) = N_2(A_*, dA_*)/dA_*$$

where

$$N_2(A_*, dA_*) = N(A_*, dA_*) - N_1(A_*, dA_*)$$
$$= N(A_*, dA_*) - f_1(A_*)\, dA_*,$$

and using formula (1) with appropriate values of D_1 and b_1 from Table 1. We find that $f_2(A_*)$ becomes the dominant component of $f(A_*)$ for $A_* \lesssim 30$ mh (Fig. 2).

We are aware of the unavoidable uncertainties in estimating $f_2(A_*)$ especially for $A_* < 10$ mh. However, we can get an insight into the nature of $f_2(A_*)$ from the three data points corresponding to the intervals 10–20, 20–30 and 30–40 mh. We find that there is a negative linear correlation between ln $f_2(A_*)$ and A_* which suggests that $f_2(A_*)$ may be of the form,

$$f_2(A_*) = D_2 \exp(-b_2 A_*). \tag{2}$$

Table 2. Properties of the component $f_2(A_*)$ with notations similar to those in Table 1.

Second component	1889–1901	1902–1913	1914–1923	1924–1933	1934–1944	1945–1954	1955–1964	1965–1976
$D_2 \pm \sigma(D_2)$ mh^{-1}	920 ± 4	833 ± 3	1536 ± 1	1400 ± 14	1300 ± 4	1255 ± 7	1636 ± 5	1306 ± 2
	(932 ± 2)	(836 ± 1)	(1536 ± 1)	(1468 ± 4)	(1306 ± 1)	(1278 ± 2)	(1643 ± 2)	(1310 ± 1)
$b_2 \pm \sigma(b_2)$ mh^{-1}	0·0712	0·0869	0·1096	0·1031	0·0844	0·0821	0·0797	0·0688
	± 0·0059	± 0·0032	± 0·0780	± 0·1401	± 0·0037	± 0·0077	± 0·0048	± 0·0025
	(0·07164	(0·03706	(0·109596	(0·1049	(0·08451	(0·08281	(0·07994	(0·06887
	± 0·00008)	± 0·00004)	± 0·000006)	± 0·0001)	± 0·00004)	± 0·00009)	± 0·00006)	± 0·00004)
$|R_2|$	0·997	0·999	1·00	0·991	0·999	0·996	0·998	0·999
	(0·997)	(0·999)	(1·00)	(0·991)	(0·999)	(0·996)	(0·998)	(0·999)
χ^2 probability (per cent)	58	72	92	25	75	48	68	79

From weighted least-square fits to this relation we determine the values of D_2 and b_2, the coefficient of correlation $|R_2|$ between In f_2 (A_*) and A_*, and probabilities of χ^2. These are presented in Table 2. These χ^2 probabilities are not as high as those for f_1 (A_*) obviously due to the uncertainties in estimating the values of N_2. However, the values of the correlation coefficient show that the form of the function f_2 (A_*) as given by equation (2) may be essentially correct.
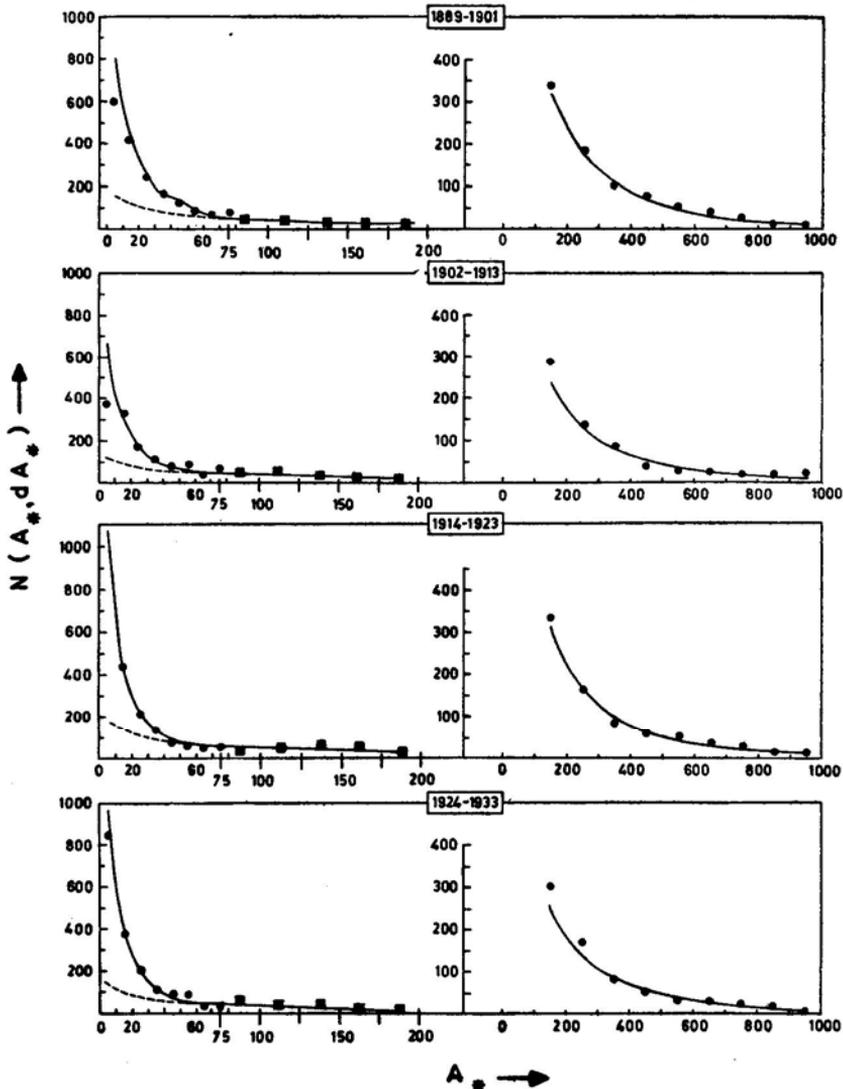
Figure 2. Comparison of theoretical and observed frequencies during the eight cycles. The continuous curve represents the formula N $(A_*,\ dA_*) = f_1(A_*)dA_*$ in the range 100–1000 mh. For $A_* < 200$ mh it represents N $(A_*,\ dA_*) = [f_1(A_*) + f_2(A_*)]\ dA_*$, The broken curve shows the value of $f_1(A_*)dA_*$ for $A_* < 80$ mh. The filled circles and squares denote the observed values of $N(A_*,\ dA_*)$ with $dA_* = 10$ mh. Filled squares have been introduced only to indicate the longer (25) interval used for determining $N(A_*,\ dA_*)$ in the range $A_* = 75$–200 mh before rescaling it to $dA_* = 10$ mh.
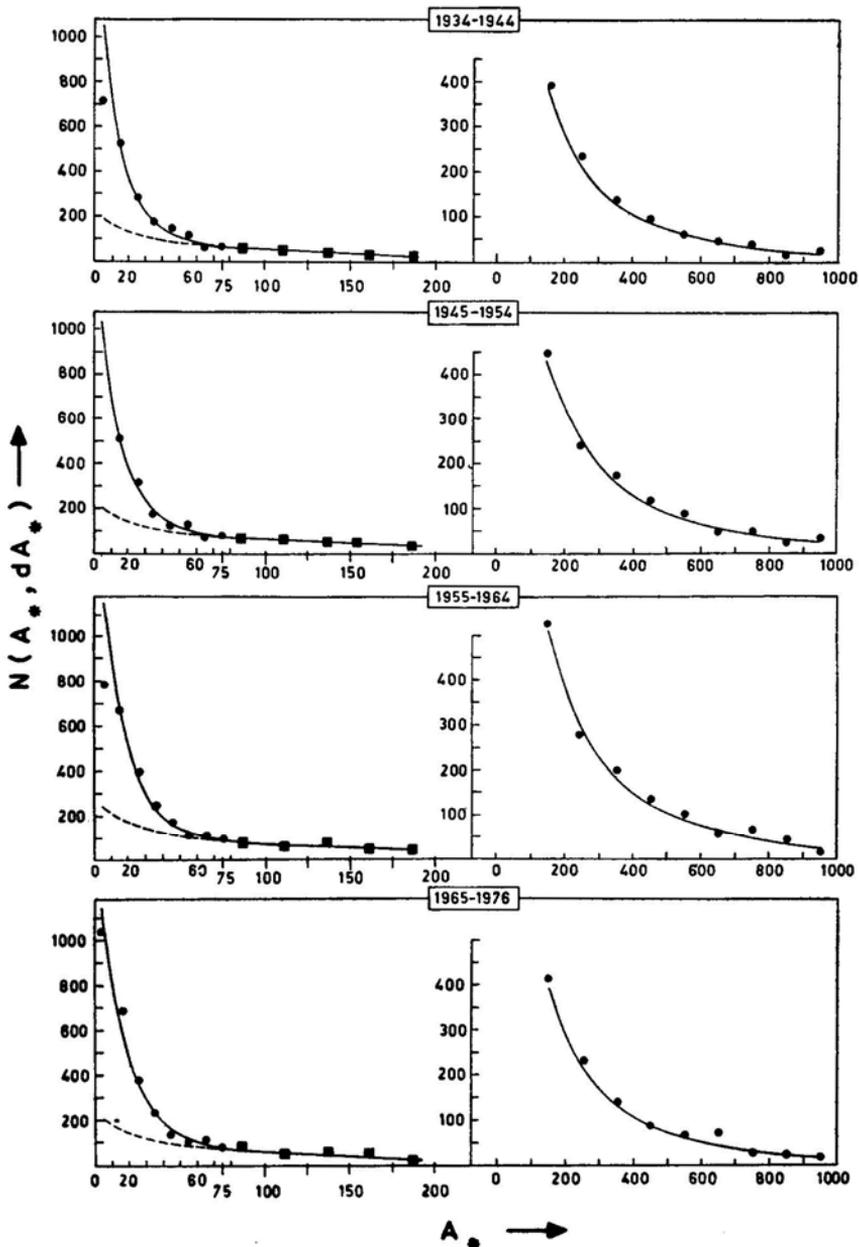
Figure 2. (Continued).

We notice that the values of b_2 –like those of b_1—are roughly constant; the mean is 0.0893 mh^{-1} and the rms deviation is $\simeq 0.0106$ mh^{-1}. This suggests that formula (2) must have some physical reality associated with it.

Summarising Section 2, we conclude that during each solar cycle the distribution $f(A_*)$ has contributions from two distinct components. The component $f_1 (A^*)$ contributes spot groups with all possible values of A_* and may be represented by

equation (1) to a high level of confidence in the domain 100–1000 mh. Although this contribution keeps increasing as A_* decreases, it becomes smaller than that of the second component f_2 (A_*) for $A_* \lesssim 30$ mh and for very small values of A_* it becomes negligible compared to f_2 (A_*). The second component seems to follow the formula given by equation (2).

It must be emphasized that our definition of the two components is different from that of the ' two populations ' described by Kuklin (1980) who has assumed the presence of two ' populations ', both represented by log-normal distribution, and has determined their proportion by placing their modes on the ' observed peaks ' in the density distribution function.

3. Difference in the physical behaviour of the two statistical components

3.1 *Variation of the Widths of the Latitude Zones*

The presence of two terms of distinct forms in $f(A_*)$ suggests that the two corresponding statistical samples of spot groups may be generated by two independent sets of flux ropes, differing in some physical or topological property related to the distribution of magnetic flux. One should, therefore, look for a significant difference in some physical property (other than area) or behaviour of the two statistical samples. The presence or absence of penumbra cannot be taken as the differentiating factor between the spot groups of the two categories, since spots of both kinds, with and without penumbra, can be found in any single large spot group belonging to either category.

It is logical to look for the difference in the *geometrical extent* over which the spot groups in the two components are distributed on the solar surface. This could be determined from the rms spread in the latitudes of spot groups in the two components. However, we have determined the actual extent from the span between the highest and the lowest latitudes at which spot groups in different specified intervals of A_* emerge during each year. In Fig. 3, we plot the total width W (sum of the latitude spans in the two hemispheres) as a function of time t in years, for spot groups in the intervals *of* A_*, 0–25, 25–100,100–200,200–500 and 500–1000 mh. From these W–t diagrams we find the following interesting features.

1. Throughout the period of the eight cycles, the W–t curve for $A_* \leqslant 25$ mh remains highest and often quite distinct from the other curves. Thus the family of flux ropes (say family II) which provides spot groups in the sample $f_2(A_*)$ must be more widely distributed in latitudes than the family of flux ropes (family I) providing the spot groups in $f_1(A_*)$

2. Near the ends of the cycles, the latitude zone for $A_* \leqslant 25$ mh suddenly expands while the latitude zones for large spot groups continue to narrow down. (Notice the horizontal arrows in Fig. 3). This illustrates the well known fact that each new cycle begins with the appearance of small spot groups at high latitudes before the end of the earlier cycle.

The narrowing of latitude zones for big spot groups represents depletion of flux ropes of family I of the old cycle. The associated sudden expansion of the latitude
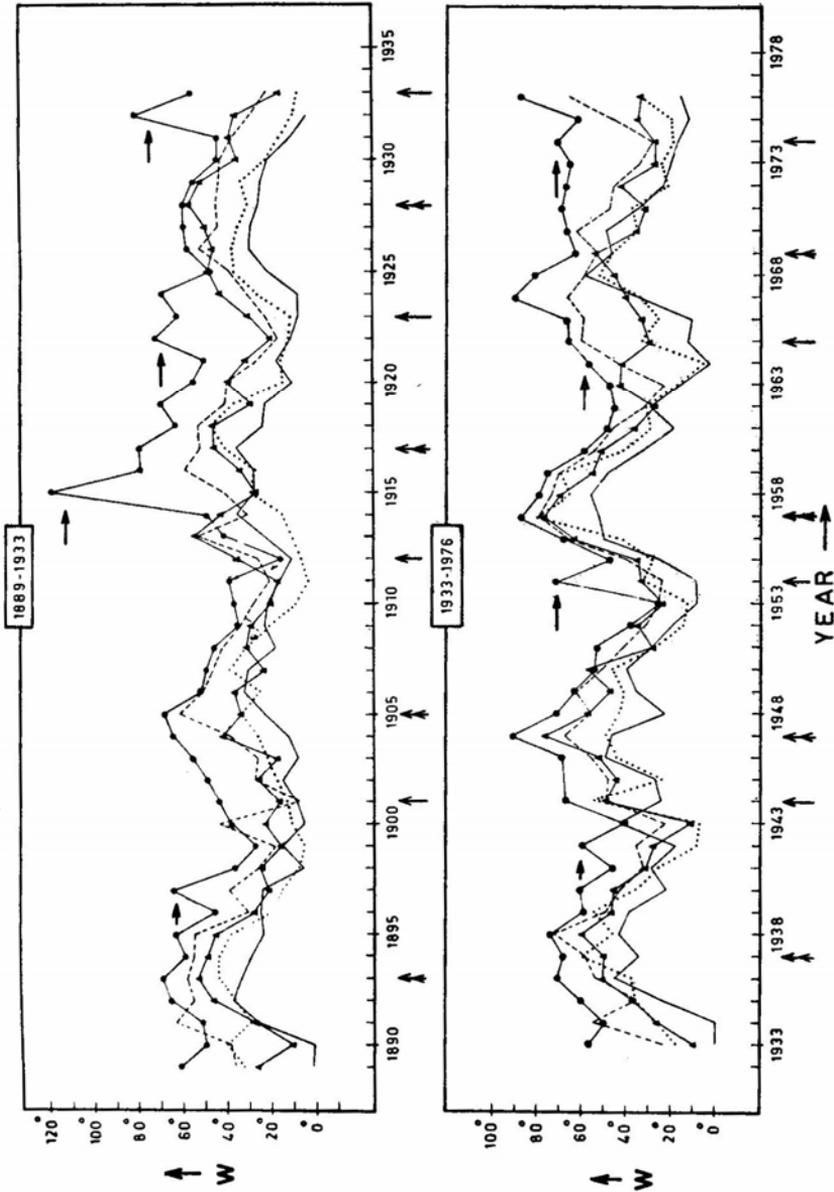
Figure 3. Total width (W) of the latitude zone corresponding to different intervals of A_*. The arrows indicate the increase of W for $A_* \leqslant 25$ mh with simultaneous decrease for high values of A_*. —●— $A_* \leqslant 25$ mh, ----- 25–100 mh, —▲— 100–200 mh, ... 200–500 mh, —— $A_* > 500$ mh. Double arrows ⇡ represent years of sunspot maximum, single arrows ↑ represent years of sunspot minimum.

zone for small spot groups represents the beginning of the emergence of family II flux ropes of the new cycle. The emergence of family I flux ropes of the new cycle may be seen to begin, as represented by expansion of the latitude zones for large spot groups, one or two years later.

3. During considerable parts of most cycles, the W–t curves are ' bunched ' in two groups and the value of A_* at which the two bunches separate vary from cycle to cycle and sometimes even within a cycle. This indicates that $f_2(A_*)$ does contribute a few spot groups to the intervals with $A_* > 25$ mh and the largest value of A_* up to which it contributes varies from cycle to cycle.

The W–t diagrams thus support the concept of the two families of flux ropes differing in latitudinal distribution and its variation.

3.2 *Relation to the Ephemeral Activity and X-ray Bright Points*

Another striking feature of the W–t curves is that in general the width of the latitude zone varies inversely as the value of A_*. Extrapolating this behaviour of W with decreasing A_* we may expect that flux tubes which are too thin even to produce
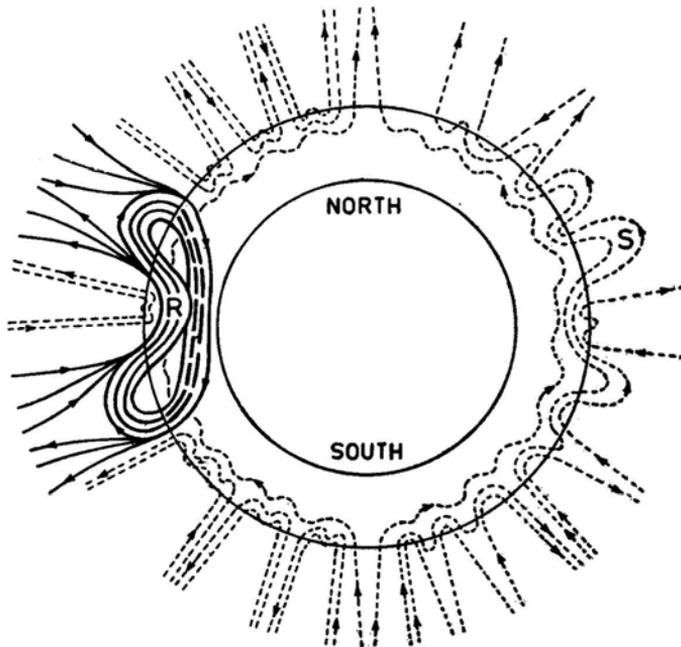
Figure 4. A schematic illustration of the phenomenological model. Thick continuous lines represent 'R family' flux ropes of the prevailing cycle provided by the faster rising parts of the newly created strong magnetic flux loops. Thick broken lines represent the slower rising parts of the same flux loops. These parts will provide the reversed global field of the next cycle. Thin dashed lines represent 'S family' flux ropes formed from the weak global field. This field is provided by the slower rising parts of the flux loops of the *previous* cycle which have diffused and dispersed all over within the convection zone while their leading parts were emerging during that cycle.

For convenience of illustration the new flux loop at only one nodal longitude is shown and the effects of the differential rotation are also omitted.

small ' pores' during their emergence, will have their latitude zone wider than that for $A_* \lesssim 25$ mh. Latitude zone of sufficiently thin flux tubes might cover even the entire sun. Ephemeral active regions and X-ray bright points provide observational evidence for the existence of such flux tubes and their emergence over the whole sun (Martin and Harvey 1979). It is interesting to note in this context that the correlation between the ephemeral activity and the annual sunspot numbers (Martin and Harvey, 1979) is consistent with the year-to-year variation of the abundance of such thin flux tubes. However, it is at present premature to seek relations of the components $f_1 (A_*)$ and $f_2 (A_*)$ with the ephemeral activity and X-ray bright points.

4. Comparison with the phenomenological model

We illustrate in Fig. 4 the phenomenological model that motivated the present study. The main aspects of the model are:

  (i)   the presence of two families of flux-tubes, S and R, both contributing to the activity of the same solar cycle (note the polarity orientations),
  (ii) a wider latitude distribution for flux tubes of family S and
  (iii) a time delay in the emergence of flux tubes of family R.

The present study brings out the existence of the two families (I and II) from observations and enables us to identify these with the families S and R of the model.

Acknowledgements

References

Gnevyshev, M. N. 1977, *Solar Phys.,* **51**, 175.
Gokhale, M. H. 1977, *Kodaikanal Obs. Bull. Ser. A., 2,* 19.
Gokhale, M. H. 1979, *Kodaikanal Obs. Bull Ser. A., 2,* 217.
Kuklin, G. V. 1980, *Bull. astr. Inst. Csl.,* **31**, 224.
Martin, S. F., Hervey, K. L. 1979, *Solar Phys.,* **64**, 93.
Lopez Arroyo, M. 1965, *Bull. astr. Inst. Csl,* **16**, 244.
Mandrykina, T. L. 1974, *Circ. astr. Obs. Lvov Univ.,* **49**,24.
Stenflo, J. O. 1976, in *IAU Symp. 71: Basic Mechanisms of Solar Activity,* Eds V. Bumba and J. Kleczek, D. Reidel, Dordrecht, p. 69.